Molecular Quantum Magnetism in LiZn$_2$Mo$_3$O$_8$

M. Mourigal,[1] W. T. Fuhrman,[1] J. P. Sheckelton,[1,2] A. Wartelle,[1,3] J. A. Rodriguez-Rivera,[4,5] D. L. Abernathy,[6]
T. M. McQueen,[1,2] and C. L. Broholm[1,4,6]

[1]*Institute for Quantum Matter and Department of Physics and Astronomy, Johns Hopkins University, Baltimore, Maryland 21218, USA*
[2]*Department of Chemistry, Johns Hopkins University, Baltimore, Maryland 21218, USA*
[3]*École Normale Supérieure de Lyon, Université de Lyon, 46 Allée d'Italie, 69364 Lyon Cedex 07, France*
[4]*NIST Center for Neutron Research, National Institute of Standards and Technology, Gaithersburg, Maryland 20899, USA*
[5]*Department of Materials Science and Engineering, University of Maryland, College Park, Maryland 20742, USA*
[6]*Quantum Condensed Matter Division, Oak Ridge National Laboratory, Oak Ridge, Tennessee 37831-6475, USA*

Inelastic neutron scattering at low temperatures $T \leq 30$ K from a powder of LiZn$_2$Mo$_3$O$_8$ demonstrates this triangular-lattice antiferromagnet hosts collective magnetic excitations from spin-1/2 Mo$_3$O$_{13}$ molecules. Apparently gapless ($\Delta < 0.2$ meV) and extending at least up to 2.5 meV, the low-energy magnetic scattering cross section is surprisingly broad in momentum space and involves one-third of the spins present above 100 K. The data are compatible with the presence of valence bonds involving nearest-neighbor and next-nearest-neighbor spins forming a disordered or dynamic state.

Insulating spin systems have demonstrated their potential to host new states of matter emerging from electronic correlations, quantum fluctuations, and entanglement [1,2]. They offer a unique and controlled avenue for quantitative comparisons between quantum many-body theory and experimental observations [3–5]. Considerable theoretical efforts are now devoted to understanding the ground state and excitations of two-dimensional antiferromagnets where spin interactions are frustrated as for the triangular and kagome lattices [6,7]. Neutron scattering investigations of materials with such lattices discovered important features associated with the concept of the quantum spin liquid [7], such as the absence of static correlations down to very low temperatures [8,9] and deconfined fractional spin excitations [10,11].

To make quantitative comparisons with theory, the sensitivity to defects and site mixing inherent to magnetic transition metal oxides is a significant challenge [12], particularly for gapless spin liquids. Beyond single-molecule magnets with purely local spin dynamics [13], spin degrees of freedom that are delocalized on stable organic molecules [14–16] or inorganic clusters [17] can host collective electronic and magnetic phenomena controlled by interactions between magnetic molecules [14–16,18–20]. Contrasting in the range and nature of interaction and disorder, different collective properties might be possible in such materials.

In this Letter, we investigate the spin dynamics of LiZn$_2$Mo$_3$O$_8$, an insulating compound where spin-1/2 carrying Mo$_3$O$_{13}$ clusters form a triangular lattice [Fig. 1(a)] with dominant antiferromagnetic interactions [17]. Our inelastic neutron scattering data from powder specimens of LiZn$_2$Mo$_3$O$_8$ provide evidence for collective molecular magnetism. We observe a low-temperature spectrum from 0.2 meV to at least 2.5 meV compatible

with the presence of valence bonds entangling nearest- and next-nearest-neighbor Mo$_3$O$_{13}$ spin clusters and spectral weight corresponding to at most 1/3 of the spins.
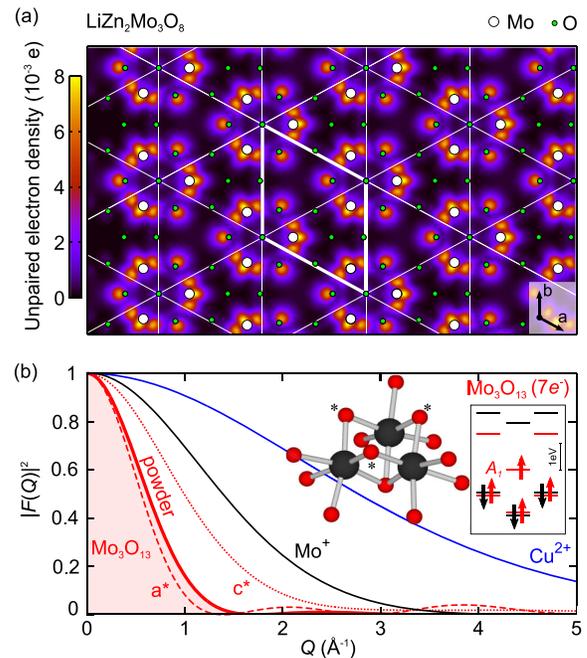
FIG. 1 (color online). (a) Triangular lattice of Mo$_3$O$_{13}$ molecules. Thick lines highlight the unit cell and the color map shows the unpaired electronic density of Mo$_3$O$_{13}$(7e) integrated along c. (b) Square of the spin-only form factor of Mo$_3$O$_{13}$(7e) (molecular orbital level diagram in the inset) calculated along a^* (dashed line), c^* (dotted line), powder averaged (solid line), and compared to that of Cu^{2+} (blue thin line) and Mo$^+$ (black thin line).

The structure of $LiZn_2Mo_3O_8$ ($Zn_2Mo_3O_8$) comprises Mo_3O_{13} clusters organized in the hexagonal ab plane of the $R\bar{3}m$ ($P6_3mc$) space group. These planes are stacked along c and separated by nonmagnetic Zn and Li ions (Zn) with six (two) layers per unit cell [17,21]. The Mo_3O_{13} units maintain $C3v$ point symmetry down to at least 12 K with an internal Mo-Mo distance $d_0 = 2.6$ Å, and a greater distance $d'_0 = 3.2$ Å between Mo atoms of adjacent clusters [17]. This results in an effective triangular lattice of Mo_3O_{13} units, Fig. 1(a), with nearest-neighbor distance $d_1 = 5.8$ Å between molecular centers. There are seven valence electrons ($7e$) per cluster in $LiZn_2Mo_3O_8$ and six ($6e$) in $Zn_2Mo_3O_8$.

Electronic structure calculations for $Mo_3O_{13}(7e)$ [17] find a single unpaired electron delocalized in a nondegenerate molecular orbital. With the point-group symmetry of Mo_3O_{13}, the wave function is primarily concentrated on molybdenum with substantial weight on three oxygen atoms [marked with asterisks in Fig. 1(b)]. This leads to a donut-shaped electron density of mean radius $\bar{r} \approx 1.5$ Å [Fig. 1(a)]. The large gap to higher-energy molecular levels suggests $Mo_3O_{13}(7e)$ carries spin $S = 1/2$ [Fig. 1(b)]. These theoretical predictions are corroborated by electron spin resonance [22] and high-temperature susceptibility [17,21] measurements on powder samples of $LiZn_2Mo_3O_8$ that are, respectively, described by an isotropic gyromagnetic tensor $g = 1.9(1)$ (with upper bounds on anisotropy $g_\perp/g_\parallel \approx 0.8$ to 1.2) and a matching effective moment $\mu_{eff} = 1.76(3)\mu_B$ [23], obtained by subtracting $\chi_0 = -137(48) \times 10^{-6}$ emu·mol^{-1}Oe^{-1} from the data of Ref. [17]. In contrast, the very small and temperature-independent susceptibility $|\chi_m| \approx |\chi_0|$ of $Zn_2Mo_3O_8$ [17,24] suggests that $Mo_3O_{13}(6e)$ is nonmagnetic.

Antiferromagnetic interactions between $Mo_3O_{13}(7e)$ spins in $LiZn_2Mo_3O_8$ are indicated by a large negative Weiss constant $\Theta_W = -339(12)$ K [23] for temperatures $T \geq 100$ K. These may be primarily ascribed to super-exchange between adjacent clusters via short Mo-O-Mo (angles 97° and 102°) paths. Below $T^* = 96$ K, the susceptibility enters another effective Curie-Weiss regime with $\Theta_W^* = -27(6)$ K and $\mu_{eff}^* = 0.94(6)\mu_B$. This corresponds to an apparent loss of 71(4)% ($\approx 2/3$) of the spins and was interpreted in Ref. [17] as a result of valence bond condensation. Despite a large $|\Theta_W|$, specific heat shows no evidence for a transition to magnetic long-range order down to 0.1 K but an upturn in the magnetic part of C_p/T from $T \approx 10$ to 0.1 K [17], consistent with a gapless magnetic excitation spectrum.

To probe the corresponding magnetic excitations, we carried out inelastic neutron scattering experiments using the MACS spectrometer [25] at the NIST Center for Neutron Research and the ARCS spectrometer [26] at the ORNL Spallation Neutron Source. Powder samples of $^7LiZn_2Mo_3O_8$ ($m = 18$ g) and $Zn_2Mo_3O_8$ ($m = 12$ g) were held in Al cans and cooled to 1.7 and 5.0 K,
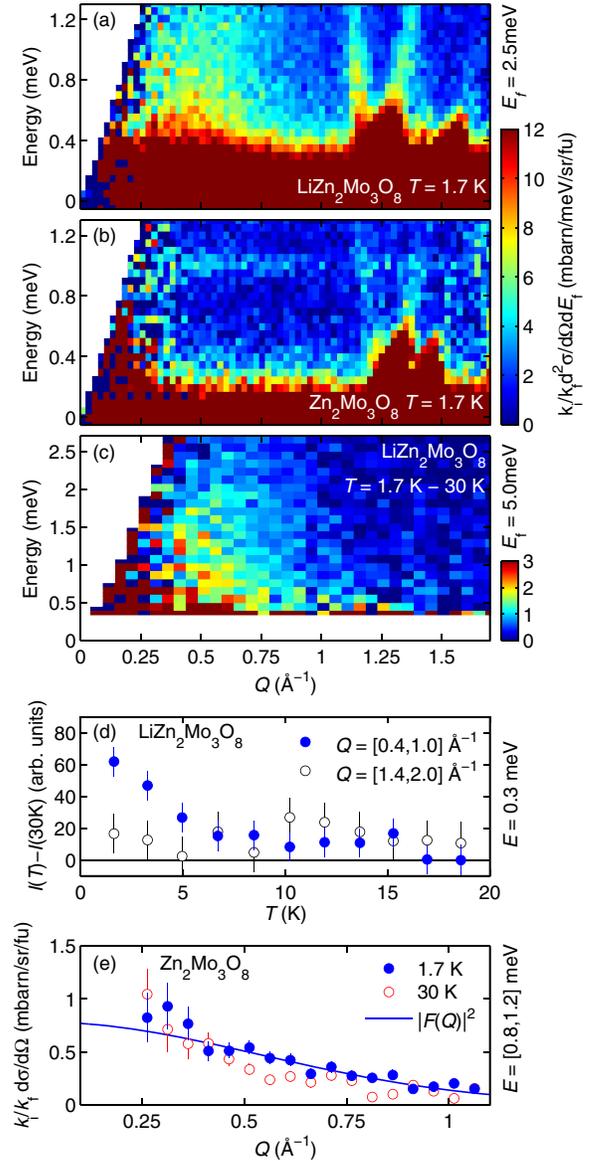
FIG. 2 (color online). Neutron scattering cross section for (a) $LiZn_2Mo_3O_8$ and (b) $Zn_2Mo_3O_8$ at 1.7 K. The intensity is normalized to absolute units corresponding to mb meV^{-1} sr^{-1} per formula unit. (c) Temperature evolution from 30 to 1.7 K in $LiZn_2Mo_3O_8$ ($E_f = 5.0$ meV). (d) Temperature evolution at $E = 0.3$ meV in $LiZn_2Mo_3O_8$ ($E_f = 3.7$ meV) comparing low Q and high Q (full and open symbols, respectively). (e) Integrated intensity of the $E = 1.0$ meV mode in $Zn_2Mo_3O_8$ for 1.7 and 30 K. The blue line is a comparison to the calculated $|F(Q)|^2$ for $Mo_3O_{13}(7e)$. Error bars represent 1 standard deviation.

respectively. The low-energy regime ($\approx \Theta_W^*$) was explored on MACS using fixed final neutron energies $E_f = 2.5, 3.7,$ and 5.0 meV and appropriate combinations of cooled Be and BeO filters before and after the sample to suppress higher-order contamination. Higher energies ($\approx \Theta_W$) were studied on ARCS configured with a fixed incident energy $E_i = 154$ meV and a chopper frequency of 600 Hz. The corresponding FWHM energy resolutions were 0.10, 0.18,

0.21, and 6.6 meV. Contributions from the empty cryostat were subtracted and the measured intensity was normalized to Bragg scattering from the sample [27].

We start with the low-energy experiment for which the cross section $\tilde{I}(Q,E) \equiv k_i/k_f(d^2\sigma/d\Omega dE_f)$ is plotted in Figs. 2(a) and 2(b) as a function of neutron energy transfer $E \equiv \hbar\omega$ and momentum transfer $\hbar Q \equiv \hbar|\mathbf{Q}|$. Besides elastic nuclear scattering, there is for $LiZn_2Mo_3O_8$ a broad plume of scattering extending from the elastic line up to the highest measured $E = 1.3$ meV, concentrated at small $Q < 1.0$ Å^{-1}, and with a temperature-dependent characteristic wave vector [Fig. 2(a)]. There is no such signal for $Zn_2Mo_3O_8$ in the same Q range, but instead a weak flat mode at $E = 1.01(1)$ meV, the intensity of which decreases with Q and vanishes by $Q \approx 1.0$ Å^{-1} [Fig. 2(b)]. For larger $Q > 1.1$ Å^{-1}, both samples display V-like ridges of intensity emerging from nuclear Bragg reflections. This spurious signal is temperature independent and results from incoherent elastic scattering from the monochromator or analyzer and a nuclear Bragg reflection from the sample.

Our observations can be compared to the cross section for inelastic magnetic neutron scattering associated with Mo_3O_{13} spins, $\tilde{I}_m(Q,E) = r_0^2|(g/2)F(Q)|^2 2\tilde{S}(Q,E)$. Here, $\tilde{S}(Q,E)$ is the dynamical spin correlation function, $F(Q)$ the spherically averaged form factor for unpaired electrons in the sample, and $r_0 = 0.539 \times 10^{-12}$ cm. Within the dipole approximation [28] and assuming a quenched orbital contribution for $Mo_3O_{13}(7e)$, we obtain the spin-only form factor $F(\mathbf{Q}) = \int d^3\mathbf{r}\rho(\mathbf{r})e^{i\mathbf{Q}\cdot\mathbf{r}}$ from the unpaired electron density $\rho(\mathbf{r})$ of Fig. 1(a).

The spherically averaged squared amplitude $|F(Q)|^2$ decreases with increasing Q and drops to 10% of its initial value by $Q \approx 1.0$ Å^{-1} [Fig. 1(b)]. This resembles the trend observed experimentally for small Q in Figs. 2(a) and 2(b), suggesting that both the broad signal in $LiZn_2Mo_3O_8$ and the flat excitation in $Zn_2Mo_3O_8$ have a magnetic origin. For $LiZn_2Mo_3O_8$ this is reinforced by the temperature evolution of the signal, determined by subtracting 30 K data from lower temperature measurements. Upon cooling to 1.7 K, the intensity increases for $Q < 1.0$ Å^{-1} and from the elastic line up to at least $E = 2.5$ meV [Fig. 2(c)]. A more detailed temperature dependence focusing on $E = 0.3$ meV reveals a substantial decrease of the $Q < 1.0$ Å^{-1} signal from $T = 1.7$ K to $T \approx 10$ K while the $Q > 1.4$ Å^{-1} is T independent [Fig. 2(d)].

In contrast, the signal observed in $Zn_2Mo_3O_8$ [Fig. 2(b)] consists of a weak resonant mode with integrated intensity that follows $|F(Q)|^2$ remarkably well, particularly for $0.4 < Q < 1.0$ Å^{-1} [Fig. 2(e)]. This flat mode carries a temperature-independent spectral weight corresponding to $\approx 10\%$ of that observed in $LiZn_2Mo_3O_8$ [Fig. 2(a)] or about 3% of that expected from one $S = 1/2$ per Mo_3O_{13} cluster. We associate this scattering with a local intramolecular excitation of $Mo_3O_{13}(6e)$ that validates the general trend of our *ab initio* predictions for the form factor [Fig. 1(b)].
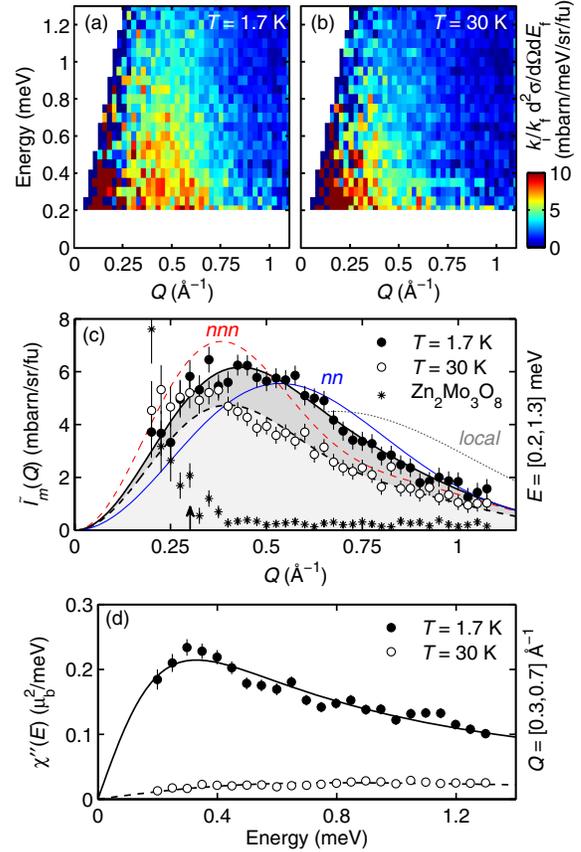
FIG. 3 (color online). Neutron scattering intensity in $LiZn_2Mo_3O_8$ ($E_f = 2.5$ meV) at (a) 1.7 K and (b) 30 K corrected for the sample incoherent scattering. (c) Momentum dependence of $\tilde{I}_m(Q)$ for $LiZn_2Mo_3O_8$ compared to $Zn_2Mo_3O_8$ ($0.2 \leq E \leq 0.8$ meV) revealing background contributions below $Q \approx 0.3$ Å^{-1} (black arrow). Fits to $\tilde{I}_{vb}(Q)$ are indicated by thick black lines (solid 1.7 K, dashed 30 K). The thin lines are fits to $\tilde{I}_d(Q)$ at 1.7 K with $d_0 = 2.6$ Å (dotted gray), $d_1 = 5.8$ Å (solid blue), and $d_2 = 10.0$ Å (dashed red). (d) Energy dependence of $\chi''(E)$ at 1.7 K (full symbols) and 30 K (open symbols). Solid and dashed lines are fits to a relaxation response. Error bars represent 1 standard deviation.

For a more quantitative understanding, we isolated the inelastic magnetic scattering contribution, $\tilde{I}_m(Q,E)$, by subtracting the sample elastic nuclear scattering. Specifically, the elastic incoherent line shape observed in $Zn_2Mo_3O_8$ for $E < 0.8$ meV and $0.3 \leq Q \leq 1.1$ Å^{-1} was scaled to the $\tilde{I}(Q, E = 0)$ intensity of $LiZn_2Mo_3O_8$ and subtracted [Figs. 3(a) and 3(b)].

The momentum dependence of the resulting intensity, $\tilde{I}_m(Q) = \int dE\tilde{I}_m(Q,E)$, was extracted by integrating over $0.2 < E < 1.3$ meV. A peak is observed for $Q = 0.41(2)$ Å^{-1} at 1.7 K, which shifts to a lower $Q = 0.35(2)$ Å^{-1} upon warming to 30 K [Fig. 3(c)]. This indicates the signal is a collective excitation of the $Mo_3O_{13}(7e)$ spins rather than a local intramolecular excitation. The latter would peak at a much higher Q,

see the dotted line in Fig. 3(c), and be temperature independent.

We modeled $\tilde{I}_m(Q)$ using the powder-averaged equal-time structure factor of a valence bond, $\tilde{I}_d(Q) \propto |F(Q)|^2[1 - \sin(Qd)/(Qd)]$, with d the distance between antiferromagnetically interacting spins. Fits to the data in the range $0.3 \leq Q \leq 1.1$ Å^{-1} with variable d (not shown) yield an effective $d^* = 7.4(2)$ Å at 1.7 K, indicating temperature-dependent correlations that are longer ranged than the nearest-neighbor spacing of 5.8 Å. Fixing d to d_1 (blue solid line) or to the next-nearest-neighbor distance $d_2 = 10.0$ Å (red dashed line) does not yield a satisfactory fit to the 1.7 K data [Fig. 3(c)]. A much better fit is obtained by allowing the superposition of valence bonds for several near neighbors $\tilde{I}_{vb}(Q) = r_0^2/6|F(Q)|^2 S_{vb}(Q)$, where $S_{vb}(Q) = \sum_{i=1}^{2} m_i^2[1 - \sin(Qd_i)/(Qd_i)]/\mu_B^2$, with m_i^2 the squared moment per formula unit entangled in a valence bond d_i. Fits to this model, shown in Fig. 3(c) for 1.7 K (solid bold line) and 30 K (dashed bold line), yield $m_1^2 = 0.10(1)\mu_B^2$ [55(9)% of $\sum_i m_i^2$] and $m_2^2 = 0.08(1)\mu_B^2$ [45(7)%] at 1.7 K and $m_1^2 = 0.03(1)\mu_B^2$ [27(11)%] and $m_2^2 = 0.09(1)\mu_B^2$ [73(15)%] at 30 K. These results are independent of the background subtraction within error bars [23]. Including a third neighbor distance d_3 does not significantly improve the fits and strongly depends on the background subtraction. While limited to low energy, our findings are consistent with the superposition of valence bonds involving first and second nearest neighbors at 1.7 K. The structure factor shifts to lower Q upon warming to 30 K, a phenomenology also observed in the kagome quantum spin liquid kapellasite [9].

The energy dependence of the signal was analyzed through the imaginary part of the dynamical susceptibility $\chi''(Q, E) = \pi(g\mu_B)^2(1 - e^{-\beta E})\tilde{S}(Q, E)$. The momentum-integrated susceptibility $\chi''(E)$ is shown in Fig. 3(d) for $0.3 < E < 0.7$ meV. There is no discernible gap or resonance and the data are well described by a relaxation response $\chi''(E) = \chi' E\Gamma/(E^2 + \Gamma^2)$ with relaxation rate $\Gamma = 0.36(1)$ meV at 1.7 K and $\Gamma = 0.91(5)$ meV at 30 K. The temperature dependence of Γ and its similarity in magnitude to $|\Theta_W^*| = 2.3(5)$ meV again point to a collective phenomenon.

The inelastic spectral weight per formula unit $m^2 = 3\mu_B^2 \iint Q^2[g^2\tilde{S}(Q, E)]dQdE/\int Q^2dQ$ can be directly compared to $\mu_{eff}^{*2} = 0.94(6)\mu_B^2$ derived from bulk susceptibility data for $20 < T < 90$ K and associated with $\approx 1/3$ of the spins. Accounting for the intensity on the neutron energy gain side and integrating over the range $0.2 < E < 1.3$ meV and $0.3 < Q < 1.1$ Å^{-1} yields $m^2 = 0.23(4)\mu_B^2$ at 1.7 K and $m^2 = 0.25(7)\mu_B^2$ at 30 K. This agrees well with $\sum_i m_i^2$ obtained above and yields $m^2 \approx 0.27\mu_{eff}^{*2}$ (and thus only $\approx 0.08\mu_{eff}^2$). The shortfall is attributed to the limited range of E integration. To overcome this, we modeled the dynamic structure factor as $g^2\tilde{S}_{th}(Q, E) = S_{vb}(Q)f(E)$, where
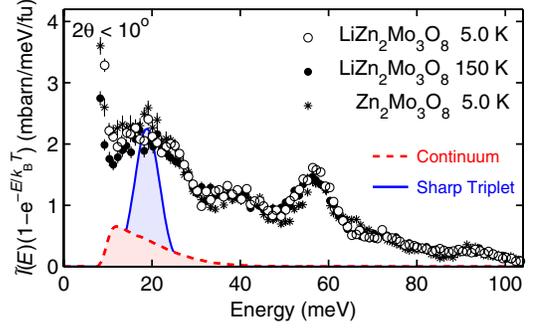
FIG. 4 (color online). Energy dependence of the neutron scattering intensity ($E_i = 154$ meV) at low scattering angles ($2\theta < 10°$) for LiZn$_2$Mo$_3$O$_8$ at 5 K (open circles) and 150 K (black circles) and Zn$_2$Mo$_3$O$_8$ at 5 K (black stars). The solid blue and dashed red lines are predictions for a sharp triplet excitation ($\Delta = J_{av}$) and continuum ($\Delta = J_{av}/2$, bandwidth $2J_{av}$), respectively. Error bars represent 1 standard deviation.

$f(E) = \mathcal{C}(T)\theta(E^* - |E|)\Gamma E/[(\Gamma^2 + E^2)(1 - e^{-\beta E})]$, with E^* a high-energy cutoff and $\mathcal{C}(T)$ a dimensionless prefactor to ensure normalization $\int f(E)dE = 1$. With the parameters from the best fits, the reconstructed spectral weight extrapolates to μ_{eff}^{*2} for a cutoff energy $E^* \approx 11$ meV, indicating that a maximum of 1/3 of the spins participate in this low-energy signal.

Searching for higher-energy spectral weight, Fig. 4 presents the energy dependence of the neutron scattering intensity $\tilde{I}(E < 100$ meV$)$ at low scattering angles ($2\theta < 10°$). The scattering is dominated by broad features centered around 20, 42, and 57 meV that are common to LiZn$_2$Mo$_3$O$_8$ and Zn$_2$Mo$_3$O$_8$. With an intensity that increases with Q [23] and varies with T in accordance with the Bose factor, they are associated with acoustic and optical phonons. Their large density of states at low energies indicates they are likely associated with Mo$_3$O$_{13}$ clusters, thus confirming the stability of these molecular units. In contrast, no magnetic signal is apparent.

Using an average exchange interaction $J_{av} = 3k_B\Theta_W/6S(S + 1) \approx 19.5$ meV, we modeled the energy dependence of $\tilde{I}_m(Q, E)$ for a singlet to triplet transition with distance d_1 and integrated spectral weight $m^2 = \mu_{eff}^2 - \mu_{eff}^{*2} = 2.20(16)\mu_B^2$ in two cases: a resolution-limited transition at $\Delta = J_{av}$ and a gapped continuum with $\Delta = J_{av}/2$ and bandwidth $2J_{av}$ [Fig. 4]. While the sharp excitation, if present, would be clearly visible at low scattering angles, the continuum mostly develops out of the kinematic range of our experiment [23] with a very weak accessible intensity, representing a fraction of the phonon contribution. While we cannot exclude a sharp excitation with $\Delta > 30$ meV, the analysis suggests the missing spectral weight may as well hide in a weak 10–40 meV continuum obscured by phonon scattering.

The magnetism of LiZn$_2$Mo$_3$O$_8$ differs radically from that of the spin-1/2 triangular lattice Heisenberg antiferromagnet, which has long-range spin order [29,30]. Along

with previously published thermomagnetic data [17], our neutron scattering data indicate a quantum fluctuating low-temperature state with low-energy excitations carrying at most a third of the spectral weight expected from the high-temperature effective moment. The low-energy spin correlations are compatible with valence bonds involving first- and second-nearest-neighbor Mo_3O_{13} clusters. The apparently gapless spectrum indicates disorder or longer-range valence bonds than are directly detectable here. Correspondingly, the absence of detectable sharp excitation at higher energies is consistent with a disordered valence bond solid or a resonating valence bond state.

Potentially relevant deviations from the Heisenberg model that may explain these results include exchange anisotropies, longer-range interactions, multispin exchange, and magnetoelasticity. Recently, a mechanism based on the cooperative rotation of Mo_3O_{13} clusters resulting in an emergent honeycomb lattice has been proposed for $LiZn_2Mo_3O_8$ [31]. Another interesting direction is Schwinger boson mean-field theory [32]. It may be possible to distinguish between these scenarios through lower Q inelastic data or by examining the magnetic field dependence of the present data.

[1] P. W. Anderson, Mater. Res. Bull. **8**, 153 (1973).
[2] P. A. Lee, Rep. Prog. Phys. **71**, 012501 (2008).
[3] M. Stone, D. Reich, C. Broholm, K. Lefmann, C. Rischel, C. Landee, and M. Turnbull, Phys. Rev. Lett. **91**, 037205 (2003).
[4] B. Lake, A. M. Tsvelik, S. Notbohm, D. Alan Tennant, T. G. Perring, M. Reehuis, C. Sekar, G. Krabbes, and B. Büchner, Nat. Phys. **6**, 50 (2009).
[5] R. Coldea, D. A. Tennant, E. M. Wheeler, E. Wawrzynska, D. Prabhakaran, M. Telling, K. Habicht, P. Smeibidl, and K. Kiefer, Science **327**, 177 (2010).
[6] Z. Hao and O. Tchernyshyov, Phys. Rev. Lett. **103**, 187203 (2009).
[7] L. Balents, Nature (London) **464**, 199 (2010).
[8] M. de Vries, J. Stewart, P. Deen, J. Piatek, G. Nilsen, H. Rønnow, and A. Harrison, Phys. Rev. Lett. **103**, 237201 (2009).
[9] B. Fåk et al., Phys. Rev. Lett. **109**, 037208 (2012).
[10] R. Coldea D. A. Tennant, A. M. Tsvelik, and Z. Tylczynski, Phys. Rev. Lett. **86**, 1335 (2001).
[11] T.-H. Han, J. S. Helton, S. Chu, D. G. Nocera, J. A. Rodriguez-Rivera, C. Broholm, and Y. S. Lee, Nature (London) **492**, 406 (2012).
[12] D. E. Freedman, T. H. Han, A. Prodi, P. Müller, Q.-Z. Huang, Yu.-S. Chen, S. M. Webb, Y. S. Lee, T. M. McQueen, and D. G. Nocera, J. Am. Chem. Soc. **132**, 16185 (2010).
[13] M. L. Baker et al., Nat. Phys. **8**, 906 (2012).
[14] M. Tamura and R. Kato, Sci. Tech. Adv. Mater. **10** 024304 (2009).
[15] F. L. Pratt, P. J. Baker, S. J. Blundell, T. Lancaster, S. Ohira-Kawamura, C. Baines, Y. Shimizu, K. Kanoda, I. Watanabe, and G. Saito, Nature (London) **471**, 612 (2011).
[16] S. J. Blundell and F. L. Pratt, J. Phys. Condens. Matter **16**, R771 (2004).
[17] J. P. Sheckelton, J. R. Neilson, D. G. Soltan, and T. M. McQueen, Nat. Mater. **11**, 493 (2012).
[18] T. Masuda, S. Takamizawa, K. Hirota, M. Ohba, and S. Kitagawa, J. Phys. Soc. Jpn. **77**, 083703 (2008).
[19] E. Canévet, B. Grenier, Y. Yoshida, N. Sakai, L.-P.Regnault, T. Goto, Y. Fujii, and T. Kawae, Phys. Rev. B **82**, 132404 (2010).
[20] H. Yamaguchi, A. Toho, K. Iwase, T. Ono, T. Kawakami, T. Shimokawa, A. Matsuo, and Y. Hosokoshi, J. Phys. Soc. Jpn. **82**, 043713 (2013).
[21] C. C. Torardi and R. E. McCarley, Inorg. Chem. **24**, 476 (1985).
[22] J. P. Sheckelton et al., arXiv:1312.0955.
[23] See Supplemental Material at http://link.aps.org/supplemental/10.1103/PhysRevLett.112.027202 for details of the Curie-Weiss analysis, valence bond fits, and $E_i = 154$ meV neutron scattering spectra.
[24] H. Abe, A. Sato, N. Tsujii, T. Furubayashi, and M. Shimoda, J. Solid State Chem. **183**, 379 (2010).
[25] J. A. Rodriguez et al., Meas. Sci. Technol. **19**, 034023 (2008).
[26] D. L. Abernathy, M. B. Stone, M. J. Loguillo, M. S. Lucas, O. Delaire, X. Tang, J. Y. Y. Lin, and B. Fultz, Rev. Sci. Instrum. **83**, 015114 (2012).
[27] G. Xu, Z. Xu, and J. M. Tranquada, arXiv:1305.5521.
[28] S. W. Lovesey, Theory of Neutron Scattering from Condensed Matter (Clarendon Press, Oxford, 1984).
[29] D. A. Huse and V. Elser, Phys. Rev. Lett. **60**, 2531 (1988).
[30] Th. Jolicoeur and J. C. Le Guillou, Phys. Rev. B **40**, 2727 (1989).
[31] Rebecca Flint and Patrick A. Lee, Phys. Rev. Lett. **111**, 217201 (2013).
[32] L. Messio, C. Lhuillier, and G. Misguich, Phys. Rev. B **83**, 184401 (2011); Phys. Rev. B**87**, 125127 (2013).